

PHYSICS

Pendellösung interferometry probes the neutron charge radius, lattice dynamics, and fifth forces

Benjamin Heacock^{1,2,3*}, Takuhiro Fujie^{4,5}, Robert W. Haun^{6,7}, Albert Henins¹, Katsuya Hirota^{4,8}, Takuya Hosobata⁵, Michael G. Huber¹, Masaaki Kitaguchi^{4,9}, Dmitry A. Pushin^{10,11}, Hirohiko Shimizu⁴, Masahiro Takeda⁵, Robert Valdillez^{2,3}, Yutaka Yamagata⁵, Albert R. Young^{2,3}

Structure factors describe how incident radiation is scattered from materials such as silicon and germanium and characterize the physical interaction between the material and scattered particles. We used neutron Pendellösung interferometry to make precision measurements of the (220) and (400) neutron-silicon structure factors and achieved a factor-of-four improvement in the (111) structure factor uncertainty. These data provide measurements of the silicon Debye-Waller factor at room temperature and the mean square neutron charge radius $\langle r_n^2 \rangle = -0.1101 \pm 0.0089$ square femtometers. Combined with existing measurements of the Debye-Waller factor and charge radius, the measured structure factors also improve constraints on the strength of a Yukawa modification to gravity by an order of magnitude over the 20 picometer-to-10 nanometer length scale range.

Neutrons, electrons, and x-rays all exhibit Pendellösung interference upon Bragg diffraction in the Laue geometry, where the Bragg planes are perpendicular to the entrance and exit faces of the crystal (Fig. 1A). The phenomenon—characterized by oscillations of diffracted intensity as a function of probe wavelength, crystal thickness, and lattice potential—was predicted by Ewald (1) and first observed in electron diffraction from MgO (2); it was later demonstrated by using x-rays (3) and neutrons (4, 5). X-ray Pendellösung studies in particular (3, 6–9) have proved an invaluable tool for measuring the electron density in silicon (10–13) and provide data that can be compared with ab initio lattice dynamical models (14). Neutron Pendellösung measurements yield information complementary to that obtained with other probes; however, achieving high precision has proven challenging.

A neutron wave propagating along the symmetry planes of a Bragg-diffracting crystal forms standing waves with integer periodicity to the Bragg planes. The neutron's kinematic momentum then depends on the incident neutron energy and the overlap of the standing wave with the crystalline potential. The detuning of the incident neutron wave into

energetically degenerate “fast” and “slow” modes creates a spatial beating period along the Bragg planes between the diffracted and transmitted intensities that may be resolved as Pendellösung oscillations. The absolute phase shift of the Pendellösung interference fringes is determined by the material's structure factor, which is specific to the radiation species and Miller indices (hkl) of the Bragg planes. For the neutron case, structure factors can be described in terms of the thermally averaged single-atom coherent elastic scattering amplitudes $b(Q) = 2me^{-W} \tilde{V}(Q)/\hbar^2$, where \hbar is the reduced Planck constant, m is the neutron mass, and $\tilde{V}(Q)$ is the Fourier transform of the neutron-atomic potential. The Debye-Waller factor (DWF; e^{-W}) accounts for the thermal motion of the atoms in the lattice, where $W = BQ^2/(16\pi^2)$ and B is determined by the mean-square thermal atomic displacement $\langle u^2 \rangle = B/(8\pi^2)$. The momentum transfer magnitude is $Q_{hkl} = (2\pi/a)\sqrt{h^2 + l^2 + k^2}$, where a is the lattice constant for a material with a cubic unit cell.

The main contribution to $b(Q)$ is the coherent nuclear scattering length, which is Q -independent. The leading-order Q -dependent contribution to $b(Q)$ (Fig. 1F) is the DWF, exhibiting a relative impact of a few percent. A determination of B can provide a benchmark for lattice dynamical models. The next-to-leading-order contribution to the Q -dependence of $b(Q)$ arises from the neutron's spherically symmetric charge distribution (which is a result of its three-quark composite structure) interacting with the very large interatomic electric fields of $\sim 10^8$ V cm⁻¹ (15). This interaction is described by the mean square neutron charge radius $\langle r_n^2 \rangle$, where $-\langle r_n^2 \rangle/6$ is the slope of the neutron electric form factor $G_E^n(Q^2)$ with respect to Q^2 at zero momentum transfer. Determinations of $\langle r_n^2 \rangle$ along with electron scattering data can be used to study the neutron's internal

charge distribution (16–18) or as a parameter in chiral effective field theory (EFT) studies of light nuclei (19). As proposed by (20), a Pendellösung interferometry determination of $\langle r_n^2 \rangle$ can weigh in on the slight tension between individual neutron scattering experiments making up the Particle Data Group (PDG)-recommended value of $\langle r_n^2 \rangle_{\text{PDG}} = -0.1161(22)$ fm² (21).

Aside from the expected B and $\langle r_n^2 \rangle$ contributions, $b(Q)$ is sensitive to interactions beyond the standard model of particle physics, often referred to as BSM interactions. BSM interactions on the atomic length scale would result in a distinctive Q -dependence (22). Yet-to-be-detected “fifth” forces arise from several BSM theories seeking to explain mysteries of modern physics, including the incompatibility of general relativity and quantum mechanics (23–25), dark matter and/or dark energy (26–30), and the smallness of neutrino masses (31). The large variety of BSM theories has motivated a multidisciplinary experimental effort to constrain the yet-undiscovered physics over the entirety of physical observation scales (35 orders of magnitude in length scale) from collider experiments at the shortest length scales and highest energies to astrophysical observations at the largest length scales and lowest energies (32).

We tabulated the measured $b(Q_{hkl})$ for silicon and used these data to (i) make a high-precision determination of B for silicon at 295.5 K, (ii) measure the neutron charge radius, and (iii) place constraints on the strength of a BSM Yukawa modification of gravity over the 20 pm-to-10 nm length scale range.

Pendellösung interference may be resolved in either the diffracted or forward-diffracted beams (Fig. 1A, K_Q and K , respectively) by rotating a crystal slab precisely about the axis perpendicular to the diffraction plane [wavelength method (5)] or perpendicular to the Bragg planes [crystal thickness method (33), used here], creating an interferogram (Fig. 1E). The interferogram is then fit to a functional form (eq. S1) to determine the phase of the oscillations, which is proportional to $b(Q)$, the neutron wavelength λ , and the thickness of the crystal slab D . We also made forward-scattering ($Q = 0$) measurements for each sample orientation using a perfect-crystal neutron interferometer, a device in which a monolithic crystal connects Bragg-diffracting “blades” that protrude from a common base (Fig. 1B) (34). The phase shift between the two interferometer paths is modulated by rotating a fused silica phase flag, creating an interferogram (Fig. 1D). The phase flag interferograms are likewise fit to a functional form (eq. S4), and the phase is extracted (34). The forward-scattering phase shift from the sample is then the difference in the fitted phase between the sample-in and sample-out of the beam (Fig. 1D) and is proportional to $b(0)$, λ , and D .

¹National Institute of Standards and Technology, Gaithersburg, MD 20899, USA. ²Department of Physics, North Carolina State University, Raleigh, NC 27695, USA. ³Triangle Universities Nuclear Laboratory, Durham, NC 27708, USA. ⁴Department of Physics, Nagoya University, Nagoya 464-8602, Japan. ⁵RIKEN Center for Advanced Photonics, RIKEN, Hirosawa 2-1, Wako, Saitama 351-0198, Japan. ⁶Institute for Physical Science and Technology, University of Maryland, College Park, MD 20742, USA. ⁷Department of Physics and Engineering Physics, Tulane University, New Orleans, LA 70118, USA. ⁸High Energy Accelerator Research Organization, Tsukuba 305-0801, Japan. ⁹Kobayashi-Maskawa Institute, Nagoya University, Nagoya 464-8602, Japan. ¹⁰Institute for Quantum Computing, University of Waterloo, Waterloo, ON N2L3G1, Canada. ¹¹Department of Physics and Astronomy, University of Waterloo, Waterloo, ON, Canada, N2L3G1
*Corresponding author. Email: benjamin.heacock@nist.gov

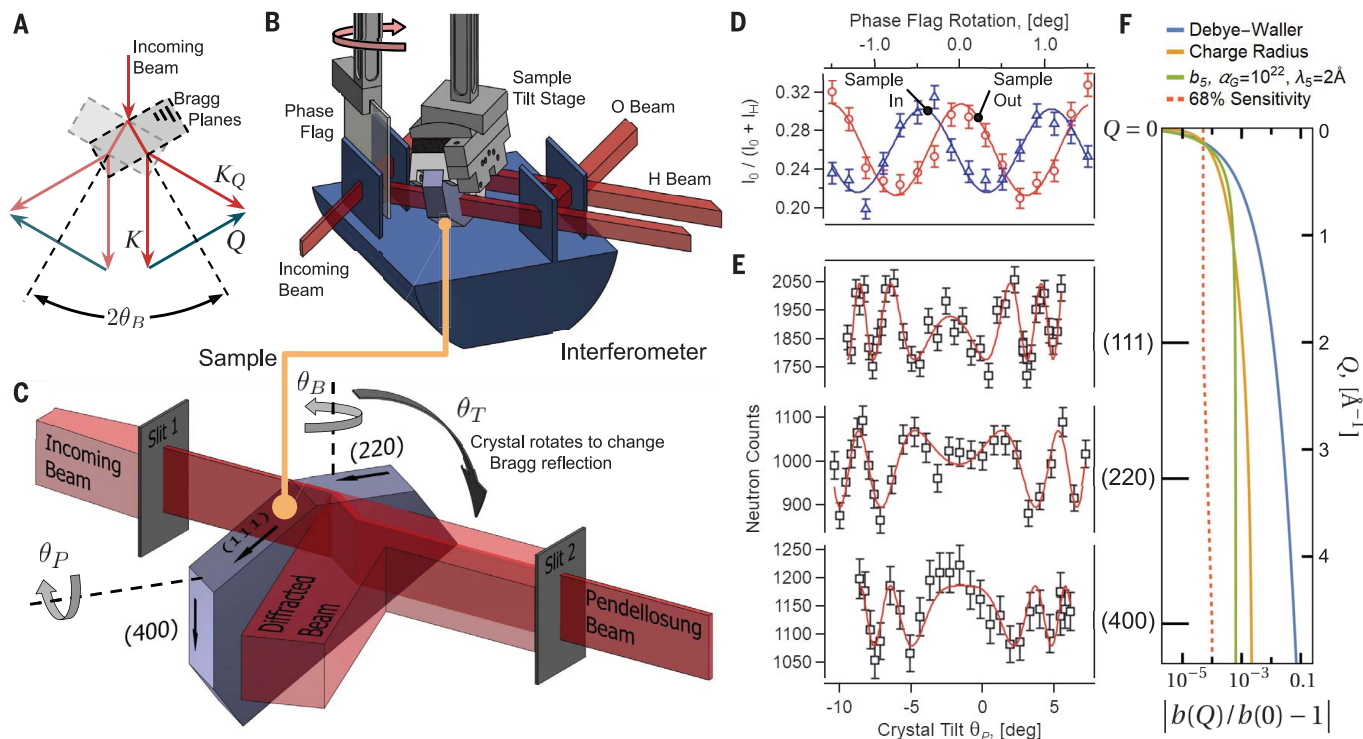


Fig. 1. Pendellösung interference in silicon. (A) Bragg diffraction Laue geometry can be measured when the crystal is rotated by $\pm\theta_B$ relative to the incoming monochromatic beam. Here, Q is the momentum transfer, and K and K_Q are the forward-diffracted and diffracted wave vectors, respectively. (B) The quantity $b(0)D$ is measured with an interferometer. (C) $b(Q)D$ is measured by using Pendellösung oscillations in the forward-diffracted beam. The (400) arrow points in the (004) direction; we indicate Miller indices with

the largest value first to emphasize that $b(Q)$ depends on the magnitude of Q . (D and E) Typical interferograms with lines of best fit for the interferometer and pendellösung setups, respectively. Error bars are from Poisson counting statistics. (F) The theoretical relative contributions of each Q -dependent term in $b(Q)$. The Debye-Waller term is negative, whereas the other two terms are positive. The data are sensitive (68% level) to features larger than the dashed line.

The extraction of $b(Q)D$ from the measured phase shift was enabled by an in situ determination of λ in which Pendellösung interferograms were obtained with the crystal rotated by both positive and negative Bragg angles $\pm\theta_B$ (Fig. 1A). The average phase shift is then quadratic in the slight difference in wavelength between the two interferograms and small enough to be neglected. The average wavelength was computed by using $\lambda = 4\pi\sin\theta_B/Q_{hkb}$, the silicon lattice constant, and $2\theta_B$ as given by an angular encoder embedded in the crystal's rotational positioning stage. A similar approach for measuring wavelength was used for the forward scattering measurements, with the interferometer and accompanying optics rotated by $\pm\theta_B$ of the interferometer.

Prior measurements of $b(Q_{111})$ were subject to strain fields in the crystal slab, observed as a one-directional phase shift with distinct wavelength dependence (35). However, the reported strain gradients were much larger than what is observed in neutron interferometers generally (36, 37) and specifically in a neutron interferometer that used a very similar machining and post-fabrication process (38) to the Pendellösung sample used here. Reducing strain gradients invariably comes

at the cost of increased variation in D , but a strain-relieving acid etch now typical for neutron interferometers was not performed in the prior measurement of $b(Q_{111})$ (35). To separate $b(Q)$ from D , we normalized the Pendellösung phase shift with the forward scattering phase shift measured over the same relevant crystal volume for each Bragg reflection. To this end, flats were cut on the Pendellösung sample so that it could fit between the interferometer optical components, with the neutron beam still illuminating the required sample area. The ratio of the two measurements forms $b(Q)/b(0)$, naturally isolating the Q -dependence of the scattering amplitude while also eliminating the need to measure D by other means. This normalization relaxes the requisite crystal flatness, enabling measurements of $b(Q)/b(0)$ using an acid-etched, strain-free crystal.

Both Pendellösung and forward scattering measurements were performed at the neutron interferometer and optics facility auxiliary beamline (NIOFa) at the National Institute of Standards and Technology (NIST) Center for Neutron Research (NCNR). The NIOFa provides both 2.2 and 4.4 Å monochromatic ($\Delta\lambda/\lambda \sim 0.5\%$) neutrons (39). The (220) and (400) Pendellösung interferograms were meas-

ured by using 2.2 Å, and the (111) Pendellösung interferograms and interferometer forward scattering measurements used 4.4 Å. The resulting ratios $b(Q)/b(0)$ for the (111), (220), and (400) Bragg reflections are reported in Table 1.

The theoretical shape versus Q of the contributions to $b(Q)/b(0)$ from the DWF and $\langle r_n^2 \rangle$ are shown in Fig. 1F. To extract these two parameters, the three measured values of $b(Q)/b(0)$ were fit to

$$b(Q)/b(0) = e^{-W} \left[1 - Z \frac{b_{ne}}{b(0)} \right] + f_e(hkl) \frac{b_{ne}}{b(0)} \quad (1)$$

by minimizing the χ^2 sum of weighted residuals, where Z is the crystal's atomic number and B and b_{ne} are treated as fit parameters. The room-temperature x-ray silicon form factors $f_e(hkl)$ in units of elementary charge are given by x-ray scattering measurements (13). The neutron-electron scattering length b_{ne} is related to the charge radius by $b_{ne} = \langle r_n^2 \rangle m_n / (3m_e a_0) = \langle r_n^2 \rangle / (86.34 \text{ fm})$, with the electron mass m_e and Bohr radius a_0 . The fit function's sensitivity to the forward scattering length $b(0)$ (40) and $f_e(hkl)$ (13) is small compared with experimental uncertainties.

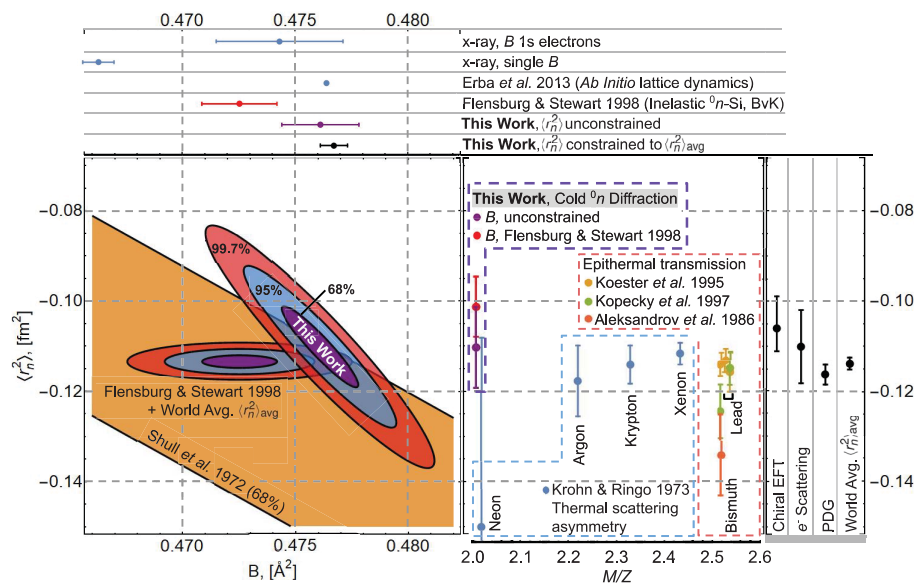


Fig. 2. Confidence regions over $\langle r_n^2 \rangle$ and B . Data have been rescaled to 295.5 K and compared with previous work. Our data are consistent with the previous (111) silicon measurement Shull *et al.* 1972 (35) but have four times the precision. The Erba *et al.* 2013 (14) determination of B is a theoretically computed value that does not have an estimated uncertainty. Other previous work includes that of Flensburg and Stewart 1998 (42), Krohn and Ringo 1973 (45), Koester *et al.* 1995 (58), Kopecky *et al.* 1997 (43), Aleksandrov *et al.* 1986 (59), as well as chiral EFT (19), e^- scattering (18), PDG (21), and world average (World Avg.) (41). A detailed discussion is provided in (41).

Table 1. Measured structure factors and uncertainties (68% confidence intervals). All results are scaled to 295.5 K.

hkl	$b(Q)/b(0) - 1$	Uncertainty statistical	Uncertainty systematic	Uncertainty total
(111)	-0.011075	3.5×10^{-5}	3.8×10^{-5}	5.1×10^{-5}
(220)	-0.030203	5.9×10^{-5}	3.6×10^{-5}	6.9×10^{-5}
(400)	-0.060596	8.0×10^{-5}	4.9×10^{-5}	9.4×10^{-5}

If B and $\langle r_n^2 \rangle$ are treated as free parameters, then our results are $B = 0.4761(17) \text{ \AA}^2$ and $\langle r_n^2 \rangle = -0.1101(89) \text{ fm}^2$ with a correlation coefficient of -0.94 ; the χ^2 -surface of B and $\langle r_n^2 \rangle$ versus prior determinations of both parameters is shown in Fig. 2. Detailed comparisons are made in (41), but of particular interest is the lattice dynamical result from fitting neutron inelastic scattering data to a Born-von Kármán (BvK) model $B_{\text{BvK}} = 0.4725(17) \text{ \AA}^2$ when scaled to 295.5 K (42) and the world average $\langle r_n^2 \rangle_{\text{avg}} = -0.1137(13) \text{ fm}^2$ from prior neutron scattering experiments, the computation of which is described in (41). The confidence region formed by B_{BvK} and $\langle r_n^2 \rangle_{\text{avg}}$ shows slight tension with our results.

In regard to $\langle r_n^2 \rangle$, most prior determinations come from epithermal neutron total transmission through lead or bismuth, with potentially correlated systematic uncertainties from solid-state and nuclear resonance effects (43). The only other type of experiment contributing

to $\langle r_n^2 \rangle_{\text{PDG}}$ and $\langle r_n^2 \rangle_{\text{avg}}$ are scattering asymmetry measurements in noble gases (44, 45). Pendellösung interferometry constitutes the only determination of $\langle r_n^2 \rangle$ that uses cold neutrons and contains entirely different systematic uncertainties compared with these previous methods (20, 46). Furthermore, a recent determination of $\langle r_n^2 \rangle_{\text{EFT}} = -0.106^{+0.007}_{-0.005} \text{ fm}^2$ from chiral EFT combined with measurements of the hydrogen-deuterium isotope shift (47) is consistent with our results and shifted in the same direction relative to $\langle r_n^2 \rangle_{\text{PDG}}$, with $\langle r_n^2 \rangle_{\text{EFT}}$ showing a 1.8σ difference with $\langle r_n^2 \rangle_{\text{PDG}}$ and a less-concerning 1.4σ difference with $\langle r_n^2 \rangle_{\text{avg}}$.

It may be possible to decrease uncertainties in the extracted $\langle r_n^2 \rangle$ by constraining B . However, the tendency for x-ray structure factor determinations of B to increasingly deviate from theory for higher-order structure factors (14, 48), as well as the disagreement between B as determined with x-rays versus neutrons, suggests a breakdown in the rigid atom ap-

proximation (41). On the other hand, neutron inelastic scattering data, as well as fully anharmonic lattice dynamical models, have shown that harmonic approximations used by the BvK and other models are insufficient for silicon's strong anharmonicity (49–51). Furthermore, the BvK model was unable to predict the measured frequencies on the phonon dispersion curves for relative uncertainties less than 0.5% (42), suggesting an inadequacy of the BvK model at this level of precision, in which case the quoted relative uncertainty for B_{BvK} of 0.34% may be too small. Whether semi-empirically fitting the interatomic force constants from other lattice dynamical models would produce better fits to neutron inelastic scattering data, and whether the resulting determination of B in turn agrees with our results, could provide a means for evaluating different thermodynamic lattice models. Because the reduced χ^2 for the BvK model fit was $\chi^2_{\text{red}} = 33.5$ (193 – 21 degrees of freedom) before the expansion of any experimental uncertainties (42), a particularly successful lattice model may be able to reduce uncertainties in B by up to a factor of $\sqrt{\chi^2_{\text{red}}} = 5.8$ relative to B_{BvK} . If the resulting 0.06% measurement of B were applied as a constraint to our evaluation of $\langle r_n^2 \rangle$, then the uncertainty thereof would be reduced to $\leq 0.004 \text{ fm}^2$.

A future test of lattice dynamical models by using Pendellösung interferometry may be achieved from the sensitivity of odd structure factors to three-phonon terms by means of the anharmonic DWF (aDWF). Of the reflections in Table 1, only the (111) reflection is affected by the aDWF and only at the 3×10^{-5} level (41). However, the contribution grows like $h \times k \times l$ (42), and a measurement of the (333) structure factor with a relative precision similar to Table 1 is capable of providing a determination of the average cubic displacement along the silicon bond direction $\langle u_{111}^3 \rangle$ at the 5% level. The near-room-temperature (288 K) $\langle u_{111}^3 \rangle$ has only been measured with 10% relative uncertainty through the “forbidden” (222) structure factor, which itself deviated from the expected T^2 temperature dependence extrapolated from higher temperatures ($>650 \text{ K}$) by a factor of two (52), suggesting that quantum zero-point anharmonic vibrations may contribute meaningfully to $\langle u_{111}^3 \rangle$ at room temperature. Pendellösung interferometry is distinctive in its capability to be extended to cryogenic temperatures to measure $\langle u_{111}^3 \rangle$ in the regime at which the anharmonic zero-point vibrations are the most relevant. This is of particular interest for silicon, given how the anharmonic force constants determine silicon's electrical properties and anomalous thermal expansion at low temperatures (51), providing motivation to measure higher-order odd $b(Q_{hkl})$ at a variety of temperatures.

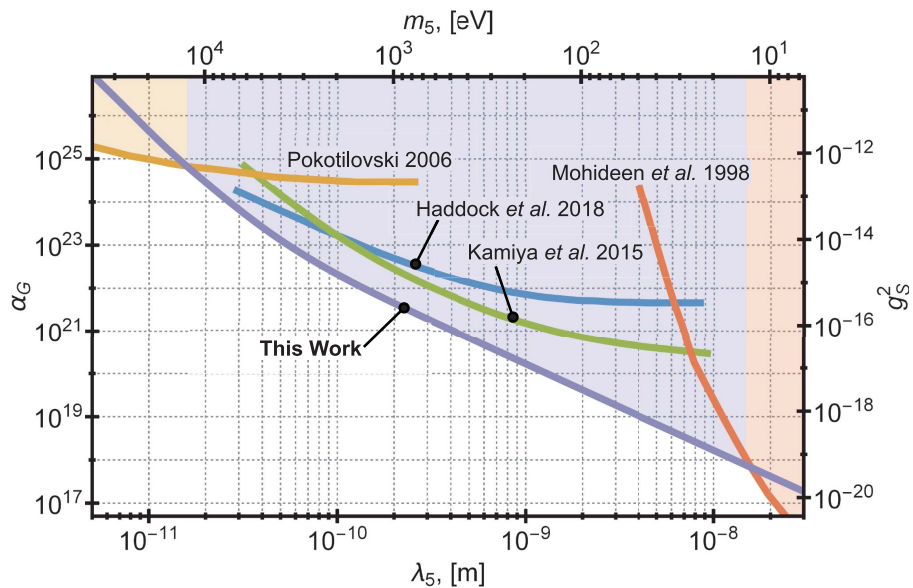


Fig. 3. Limits (95% confidence) on the strength of a Yukawa modification to gravity α_G compared with previous experiments as a function of the force's range λ_5 . The same limits constrain the coupling to nucleon number g_5^2 of a yet-undiscovered scalar with mass m_5 . The shaded region is excluded. Other limits shown are those of Pokotilovski 2006 (56), Mohideen *et al.* 1998 (60), Haddock *et al.* 2018 (55), and Kamiya *et al.* 2015 (54).

A BSM “fifth” fundamental force or other BSM physics adds an additional term

$$\delta \left[\frac{b(Q)}{b(0)} \right] = e^{-w} \frac{b_5(Q) - b_5(0)}{b(0)} \quad (2)$$

to Eq. 1, given a BSM contribution to the neutron-atomic potential $b_5(Q) = 2m\tilde{V}_5(Q)/\hbar^2$. The method for using neutron structure factors to constrain BSM physics is general: A χ^2 sum of weighted residuals for the measured structure factors—as well as B , the aDWF, and $\langle r_n^2 \rangle$ —is minimized with respect to BSM model parameters, given a functional form of $b_5(Q)$. The weights and values assigned to the B , $\langle r_n^2 \rangle$, and the aDWF residuals are to be based on an estimation of how the BSM physics would bias the experiments from which the residuals are derived. The tabulated structure factors can thus continue to constrain future BSM theories as they are developed, with improved constraints as the number of measured structure factors increases.

A common parameterization for constraining BSM physics is a Yukawa modification to gravity (24), leading to $\delta[b(Q)/b(0)]e^w = \alpha_G(3.9 \times 10^{-27} \text{ \AA}^{-2} \lambda_5^2)Q^2\lambda_5^2/(1 + Q^2\lambda_5^2)$ for the case of silicon in Eq. 2 (22); this expression depends on an interaction strength relative to gravity α_G and length scale λ_5 . The coupling to nucleon number g_5 of an undiscovered massive scalar with particle mass $m_5 = \hbar/(c\lambda_5)$, where c is the speed of light, proposed by a number of BSM theories is constrained by the same limits (24, 25, 53). The constraints

on the strength of an undiscovered Yukawa potential over the relevant range of λ_5 from this work compared with previous experiments is shown in Fig. 3. Our results constitute an order-of-magnitude improvement over nearly three decades in λ_5 . Previous limits constrain $\langle r_n^2 \rangle$ according to the PDG value and uncertainty (54, 55), except for a higher-energy experiment that uses an expanded uncertainty (56), in which a systematic shift in the measured $\langle r_n^2 \rangle$ from an unaccounted-for Yukawa modification to gravity could be relevant for $\lambda_5 \leq 10$ pm. In keeping with other previously published constraints, we likewise set the $\langle r_n^2 \rangle$ residual according to the PDG value and uncertainty when computing the limits in Fig. 3. In addition to measuring $b(Q)$ for higher-order reflections in silicon, measuring multiple $b(Q)$ from germanium, for which precision measurements only exist for the (111) reflection (57), is expected to improve constraints on α_G by a factor of five, regardless of whether $\langle r_n^2 \rangle$ is constrained because of the differing M/Z for germanium and silicon. Germanium measurements would also reduce the uncertainty in our measured $\langle r_n^2 \rangle$ to $\sim 0.005 \text{ fm}^2$ with B from both atomic species unconstrained, in which case Pendellösung interferometry could weigh in more strongly on the $\langle r_n^2 \rangle$ landscape. If determinations of B for silicon and germanium can be achieved at the 0.1% level by using neutron inelastic scattering and lattice dynamical models, then an achievable uncertainty for $\langle r_n^2 \rangle$ from Pendellösung interferometry of 0.002 fm^2 would be comparable with the

uncertainty of $\langle r_n^2 \rangle_{\text{PDG}}$. Ultimately, whereas x-ray structure factors in silicon as large as (12120) and (880) have been measured at room and liquid-nitrogen temperatures, respectively (12, 13), an expanding set of tabulated neutron structure factors for silicon, germanium, and other crystals at multiple temperatures would provide increasingly sensitive measures of material-specific thermal displacement parameters and the neutron charge radius while continuing to improve BSM constraints.

REFERENCES AND NOTES

- P. P. Ewald, *Ann. Phys.* **354**, 1–38 (1916).
- R. D. Heidenreich, *Phys. Rev.* **62**, 291–292 (1942).
- N. Kato, A. Lang, *Acta Crystallogr.* **12**, 787–794 (1959).
- D. Sippel, K. Kleinstück, G. Schulze, *Phys. Lett.* **14**, 174–175 (1965).
- C. Shull, *Phys. Rev. Lett.* **21**, 1585–1589 (1968).
- H. Hattori, Hideo Kuriyama, T. Katagawa, N. Kato, *J. Phys. Soc. Jpn.* **20**, 988–996 (1965).
- S. Tanemura, N. Kato, *Acta Crystallogr. A* **28**, 69–80 (1972).
- M. Wada, N. Kato, *Acta Crystallogr. A* **33**, 161–168 (1977).
- M. Deutsch, M. Hart, *Acta Crystallogr. A* **41**, 48–55 (1985).
- B. Willis, *Acta Crystallogr. A* **25**, 277–300 (1969).
- P. Aldred, M. Hart, *Proc. R. Soc. London Ser. A* **332**, 223–238 (1973).
- M. Spackman, *Acta Crystallogr. A* **42**, 271–281 (1986).
- S. Cummings, M. Hart, *Aust. J. Phys.* **41**, 423 (1988).
- A. Erba, M. Ferrabone, R. Orlando, R. Dovesi, *J. Comput. Chem.* **34**, 346–354 (2013).
- V. Fedorov *et al.*, *Phys. Lett. B* **694**, 22–25 (2010).
- T. R. Gentile, C. Crawford, *Phys. Rev. C Nucl. Phys.* **83**, 055203 (2011).
- H. Atac, M. Constantinou, Z.-E. Mezirani, M. Paolone, N. Sparveris, *Eur. Phys. J. A* **57**, 65 (2021).
- H. Atac, M. Constantinou, Z.-E. Mezirani, M. Paolone, N. Sparveris, *Nat. Commun.* **12**, 1759 (2021).
- E. Epelbaum, H. Krebs, P. Reinert, *Front. Phys.* **8**, 98 (2020).
- J.-M. Sparenberg, H. Leeb, *Phys. Rev. C Nucl. Phys.* **66**, 055210 (2002).
- M. Tanabashi *et al.*, *Phys. Rev. D* **98**, 030001 (2018).
- G. L. Greene, V. Gudkov, *Phys. Rev. C Nucl. Phys.* **75**, 015501 (2007).
- N. Arkani-Hamed, S. Dimopoulos, G. Dvali, *Phys. Rev. D Part. Fields* **59**, 086004 (1999).
- E. G. Adelberger, B. R. Heckel, A. E. Nelson, *Annu. Rev. Nucl. Part. Sci.* **53**, 77–121 (2003).
- V. M. Mostepanenko, G. L. Klimchitskaya, *Universe* **6**, 147 (2020).
- A. Zee, *Phys. Lett. B* **594**, 8–12 (2004).
- P. Fayet, *Phys. Rev. D Part. Fields Gravit. Cosmol.* **75**, 115017 (2007).
- S. Fichtel, *Phys. Rev. Lett.* **120**, 131801 (2018).
- P. Brax, S. Fichtel, G. Pignol, *Phys. Rev. D* **97**, 115034 (2018).
- P. Brax, S. Fichtel, P. Tanedo, *Phys. Lett. B* **798**, 135012 (2019).
- N. Arkani-Hamed, S. Dimopoulos, *Phys. Rev. D Part. Fields* **65**, 052003 (2002).
- J. Murata, S. Tanaka, *Class. Quantum Gravity* **32**, 033001 (2015).
- V. Somenkov, S. S. Shilstein, N. Belova, K. Utemisov, *Solid State Commun.* **25**, 593–595 (1978).
- H. Rauch, S. A. Werner, *Neutron Interferometry: Lessons in Experimental Quantum Mechanics, Wave-particle Duality, and Entanglement*, vol. 12 (Oxford Univ. Press, 2015).
- C. Shull, J. Oberteuffer, *Phys. Rev. Lett.* **29**, 871–874 (1972).
- B. Heacock *et al.*, *Phys. Rev. A* **95**, 013840 (2017).
- B. Heacock *et al.*, *Rev. Sci. Instrum.* **89**, 023502 (2018).
- B. Heacock *et al.*, *Acta Crystallogr. A Found. Adv.* **75**, 833–841 (2019).
- C. Shahi *et al.*, *Nucl. Instrum. Methods Phys. Res. A* **813**, 111–122 (2016).
- A. Ioffe *et al.*, *Phys. Rev. A* **58**, 1475–1479 (1998).
- Materials and methods are available as supplementary materials.

42. C. Flensburg, R. F. Stewart, *Phys. Rev. B Condens. Matter Mater. Phys.* **60**, 284–291 (1999).
43. S. Kopecky et al., *Phys. Rev. C Nucl. Phys.* **56**, 2229–2237 (1997).
44. V. Krohn, G. Ringo, *Phys. Rev.* **148**, 1303–1311 (1966).
45. V. Krohn, G. Ringo, *Phys. Rev. D Part. Fields* **8**, 1305–1307 (1973).
46. J.-M. Sparenberg, H. Leeb, *J. Electron Spectrosc. Relat. Phenom.* **129**, 315–317 (2003).
47. A. A. Filin et al., *Phys. Rev. Lett.* **124**, 082501 (2020).
48. M. Deutsch, M. Hart, P. Sommer-Larsen, *Phys. Rev. B Condens. Matter* **40**, 11666–11669 (1989).
49. O. Hellman, I. A. Abrikosov, *Phys. Rev. B Condens. Matter Mater. Phys.* **88**, 144301 (2013).
50. D. Kim et al., *Phys. Rev. B Condens. Matter Mater. Phys.* **91**, 014307 (2015).
51. D. S. Kim et al., *Proc. Natl. Acad. Sci. U.S.A.* **115**, 1992–1997 (2018).
52. J. Roberto, B. Batterman, D. Keating, *Phys. Rev. B* **9**, 2590–2599 (1974).
53. V. Nesvizhevsky, G. Pignol, K. Protasov, *Phys. Rev. D Part. Fields Gravit. Cosmol.* **77**, 034020 (2008).
54. Y. Kamiya, K. Itagaki, M. Tani, G. N. Kim, S. Komamiya, *Phys. Rev. Lett.* **114**, 161101 (2015).
55. C. C. Haddock et al., *Phys. Rev. D* **97**, 062002 (2018).
56. Y. N. Pokotilovski, *Phys. Lett. B* **719**, 341–345 (2013).
57. C. Shull, W. Shaw, *Z. Naturforsch. A* **28**, 657–661 (1973).
58. L. Koester et al., *Phys. Rev. C Nucl. Phys.* **51**, 3363–3371 (1995).
59. Y. Aleksandrov, M. Vrana, G. Manrique, T. Machekhina, L. Sedlakova, *Sov. J. Nucl. Phys.* **44**, 900 (1986).
60. U. Mohideen, A. Roy, *Phys. Rev. Lett.* **81**, 4549–4552 (1998).
61. B. Heacock, M. Huber, Open data for “Pendellösung interferometry probes the neutron charge radius, lattice dynamics, and fifth forces”. Zenodo (2021). doi:10.5281/zenodo.5080965.

ACKNOWLEDGMENTS

We thank the NIST Center for Neutron Research for providing the neutron facilities used in this work. **Funding:** This work was supported by The National Institute of Standards and Technology, the US Department of Energy (DOE) under grants 89243019SSCO00025 and DE-FG02-97ER41042, the National Science Foundation (NSF) under grant PHY-1307426, the Natural Sciences and Engineering Council of Canada (NSERC) Discovery program, and the Canada First Research Excellence Fund (CFREF). **Author contributions:** B.H., M.G.H., H.S., and A.R.Y. conceived the project. B.H., T.F., R.W.H., M.G.H., D.A.P., and R.V. collected

neutron data under the supervision of M.G.H.; A.H. performed the sample crystallographic alignment and initial fabrication. T.F., T.H., M.T., and Y.Y. machined and characterized the sample surfaces under the supervision of Y.Y.; B.H., M.G.H., and D.A.P. chemically etched the sample. M.G.H., K.H., M.K., H.S., Y.Y., and A.R.Y. were responsible for overall supervision. B.H. performed the main analysis and wrote the manuscript, with input from all authors. **Competing interests:** The authors declare no competing interests. **Data and materials availability:** The datasets and analysis code are available through Zenodo (61).

SUPPLEMENTARY MATERIALS

<https://science.org/doi/10.1126/science.abc2794>
Materials and Methods
Supplementary Text
Figs. S1 to S5
Tables S1 and S2
References (62–67)

8 June 2020; resubmitted 3 March 2021
Accepted 6 August 2021
10.1126/science.abc2794

Pendellösung interferometry probes the neutron charge radius, lattice dynamics, and fifth forces

Benjamin Heacock Takuhiro Fujiie Robert W. Haun Albert Henins Katsuya Hirota Takuya Hosobata Michael G. Huber Masaaki Kitaguchi Dmitry A. Pushin Hirohiko Shimizu Masahiro Takeda Robert Valdillez Yutaka Yamagata Albert R. Young

Science, 373 (6560), • DOI: 10.1126/science.abc2794

Setting bounds on a fifth force

Some extensions to the Standard Model of particle physics posit the existence of a fifth force to complement the existing four fundamental forces. To set bounds on the strength of such an interaction, experiments on vastly different length scales have been performed. Heacock *et al.* used an unusual method called Pendellösung interferometry to measure the neutron structure factors of silicon. The momentum dependence of the structure factors enabled the researchers to put more stringent bounds on the strength of a type of fifth force called the Yukawa force, as well as measure the charge radius of the neutron. —JS

View the article online

<https://www.science.org/doi/10.1126/science.abc2794>

Permissions

<https://www.science.org/help/reprints-and-permissions>

Use of think article is subject to the [Terms of service](#)

Science (ISSN) is published by the American Association for the Advancement of Science. 1200 New York Avenue NW, Washington, DC 20005. The title *Science* is a registered trademark of AAAS.

Copyright © 2021 The Authors, some rights reserved; exclusive licensee American Association for the Advancement of Science. No claim to original U.S. Government Works